



1 **The added value of brightness temperature assimilation for the**  
2 **SMAP Level-4 surface and root-zone soil moisture analysis over**  
3 **mainland China**

4 Jianxiu Qiu<sup>1,2</sup>, Jianzhi Dong<sup>3</sup>, Wade T. Crow<sup>3</sup>, Xiaohu Zhang<sup>4,5</sup>, Rolf H. Reichle<sup>6</sup>, Gabrielle J.  
5 M. De Lannoy<sup>7</sup>

6 <sup>1</sup>Guangdong Provincial Key Laboratory of Urbanization and Geo-simulation, School of Geography and Planning, Sun  
7 Yat-sen University, Guangzhou, 510275, China

8 <sup>2</sup>Southern Laboratory of Ocean Science and Engineering (Guangdong, Zhuhai), Zhuhai, 519000, China

9 <sup>3</sup>USDA ARS Hydrology and Remote Sensing Laboratory, Beltsville, MD 20705, USA

10 <sup>4</sup>National Engineering and Technology Center for Information Agriculture, Nanjing Agricultural University, Nanjing,  
11 China

12 <sup>5</sup>Jiangsu Key Laboratory for Information Agriculture, Nanjing Agricultural University, Nanjing, China

13 <sup>6</sup>Global Modeling and Assimilation Office, NASA Goddard Space Flight Center, Greenbelt, MD, USA

14 <sup>7</sup>Department of Earth and Environmental Sciences, KU Leuven, Heverlee, Belgium

15

16 *Correspondence to:* Jianxiu Qiu (qiujianxiu@mail.sysu.edu.cn)



17 **Abstract.** The Soil Moisture Active Passive (SMAP) Level-4 Surface Soil Moisture and Root-Zone Soil Moisture (L4)

18 product provides global estimates of surface soil moisture (SSM) and root-zone soil moisture (RZSM) via the

19 assimilation of SMAP brightness temperature (T<sub>b</sub>) observations into the Catchment Land Surface Model (CLSM).

20 Here, using in-situ measurements from 2474 sites in mainland China, we evaluate the performance of soil moisture

21 estimates from L4 and from a baseline “open-loop” (OL) simulation of CLSM without T<sub>b</sub> assimilation. Using random

22 forest regression, the efficiency of the L4 data assimilation (DA) system (i.e., the performance improvement in L4

23 relative to OL) is attributed to 8 control factors related to the land surface modelling (LSM) and radiative transfer

24 modeling (RTM) components of the L4 system. Results show that 77% of the 2287 9-km EASE grid cells in mainland

25 China that contain at least one ground station exhibit an increase in the Spearman rank correlation skill (*R*) with in-

26 situ measurements for L4 SSM compared to that of OL, with an average *R* increase of approximately 14% ( $\Delta R =$

27 0.056). RZSM skill is improved for about the same percentage of 9-km EASE grid cells, but the average *R* increase

28 for RZSM is only 7% ( $\Delta R = 0.034$ ). Results further show that the SSM DA efficiency is most strongly related to the

29 error in T<sub>b</sub> observation space, followed by the error in precipitation forcing and microwave soil roughness. For RZSM

30 DA efficiency, the three dominant control factors remain the same, although the importance of soil roughness exceeds

31 that of the T<sub>b</sub> error. For the skill of the L4 and OL estimates themselves, the top control factors are the precipitation

32 error and the SSM-RZSM coupling strength error (in descending order of factor importance for *R*<sub>OL</sub>), both of which

33 are related to the LSM component of the L4 system. Finally, we find that the L4 system can effectively filter out errors

34 in precipitation. Therefore, future development of the L4 system should focus on improving the characterization of the

35 SSM-RZSM coupling strength.

36

37 **Keywords.** SMAP Level 4, soil moisture, data assimilation, attribute analysis, random forest regression

## 38 1 Introduction

39 Soil moisture modulates water and energy feedbacks between the land surface and the lower atmosphere by

40 determining the partitioning of incoming net radiation into latent and sensible heat (Seneviratne et al., 2010, 2013).

41 High-quality, global-scale soil moisture products have become increasingly available in recent years (Gruber et al.,

42 2020). In particular, the L-band NASA Soil Moisture Active Passive (SMAP) satellite mission (Entekhabi et al., 2010;

43 Piepmeier et al., 2017) has significantly improved the skill of available, global-scale soil moisture products. However,

44 the SMAP observations contain temporal data gaps and are only representative of conditions within the top 5 cm

45 the vertical soil moisture column. To address these limitations, the SMAP Level-4 Surface and Root-Zone Soil

46 Moisture (L4) algorithm assimilates SMAP brightness temperature (T<sub>b</sub>) observations into the NASA Catchment Land

47 Surface Model (CLSM) to derive an analysis of surface (0–5 cm) and root-zone (0–100 cm) soil moisture estimates

48 with global, 3-hourly coverage (Reichle et al., 2017a; Reichle et al., 2017b; Reichle et al., 2019).



49 However, the performance of a land data assimilation (DA) system is sensitive to its parameterization and requires  
50 careful assessment. For instance, Reichle et al. (2008) demonstrate that DA based on incorrect assumptions of modeling  
51 and observation errors can degrade soil moisture estimates, compared with the case of not performing any DA.  
52 Theoretically, the optimality of DA can be evaluated using so-called innovations, or observations-minus-forecast  
53 residuals; however, an investigation of the innovations alone is often insufficient to determine if the soil moisture  
54 analysis is optimal (Crow and Van Loon, 2006).

55 Recently, Dong et al. (2019a) proposed a novel statistical framework for evaluating the performance of a soil moisture  
56 DA system. Specifically, they demonstrated that the relative skill of surface soil moisture (SSM) estimates acquired  
57 with and without DA can be estimated using the ratio of their correlations with just one noisy but independent ancillary  
58 remote sensing product. This approach was applied to the SMAP L4 system using ASCAT soil moisture retrievals.  
59 Their results show that the added value of SMAP DA is closely related to both rain gauge and vegetation density.  
60 However, due to the limited availability of independent root-zone soil moisture (RZSM) products for performing  
61 statistical error estimation, this method is only applicable for SSM estimates.

62 Relative to SSM, the efficiency of assimilating land surface observations to improve RZSM is complicated by model  
63 structural error that affects the ability of the DA to update unobserved model states. For instance, Kumar et al. (2009)  
64 identified the surface–root zone coupling strength, which is the result of a model-dependent representation of processes  
65 related to the partitioning of rainfall into infiltration, runoff, and evaporation components, as an important factor for  
66 determining RZSM improvement associated with the assimilation of SSM retrievals. Their synthetic experiments  
67 suggest that – faced with unknown true subsurface physics – overestimating the surface–root zone coupling in the land  
68 model is a more robust strategy for obtaining skill improvements in the root zone than under-estimating the coupling.  
69 Likewise, Chen et al. (2011) suggested that their Soil and Water Assessment Tool significantly under-predicts the  
70 magnitude of vertical soil water coupling in the Cobb Creek Watershed in southwestern Oklahoma, USA, and this lack  
71 of coupling impedes the ability of DA to effectively update deep-layer soil moisture, groundwater flow and surface  
72 runoff. In the context of the present paper, the evaluation of L4 RZSM estimates has been limited to relatively few  
73 SMAP core validation and sparse network sites (Reichle et al., 2017a; Reichle et al., 2017b; Reichle et al., 2019). With  
74 such limited sample sizes, the RZSM skill of the L4 product at the global scale remains uncertain.

75 The primary objective of this study is to determine the DA efficiency, i.e., performance improvement in DA results  
76 relative to the open-loop (OL) baseline of the L4 product, as a function of a variety of system aspects, including errors  
77 in CLSM forcing (e.g., precipitation), errors in key CLSM parameters (e.g., relating to vegetation), mean errors in  
78 CLSM structure (e.g., surface and root-zone coupling), and errors in the radiative transfer modeling (RTM) that links  
79 the modeled soil moisture and temperature estimates to the observed  $T_b$ .

80 To this end, we first evaluate the performance of L4 SSM and RZSM estimates using a very large number ( $n = 2474$ )  
81 of soil moisture measurement sites (generally acquired at sub-surface depths between 10 and 50 cm) within  
82 mainland China. The in-situ measurements are used to assess the DA efficiency of the L4 system, which is defined



83 as the skill difference between the L4 estimates and model-only estimates derived without SMAP Tb assimilation.  
84 Additionally, we apply a machine-learning technique to quantify by how much various control factors drive the spatial  
85 variations in the efficiency of the L4 system. In this way, we seek to prioritize future enhancements to the L4 system.

## 86 **2 Data and Methods**

87 This section briefly describes the SMAP L4 soil moisture product (Section 2.1), the extensive network of in-situ soil  
88 moisture observations over mainland China (Section 2.2) and the ancillary data sources and datasets used in the skill  
89 assessment (Sections 2.3 and 2.4). Next, we introduce the double instrumental variable (IVd) method employed to  
90 determine the errors in control factors that cannot be determined using ground observations (Section 2.5). Finally, we  
91 describe the random forest (RF) regression method used to identify the main factor(s) (out of the 8 control factors from  
92 both CLSM and RTM aspects) that affect the spatial variations in SMAP L4 DA efficiency and L4 performance  
93 (Section 2.6).

### 94 **2.1 SMAP L4 soil moisture product**

95 The SMAP L4 soil moisture product (version 4; Reichle et al., 2019) is generated by assimilating the SMAP L1C  
96 Radiometer half-orbit 36 km EASE-Grid brightness temperature (Tb) observations (Version 4 SPL1CTB; Chan et al.,  
97 2016) into the CLSM. The SMAP Tb observations are assimilated at 3-h intervals using a spatially distributed, 24-  
98 member ensemble Kalman filter (Reichle et al. 2017b). The surface meteorological forcing data are from the global  
99 Goddard Earth Observing System (GEOS) Forward Processing atmospheric analysis (Lucchesi, 2013), with  
100 precipitation corrected using the daily, 0.5-degree, gauge-based Climate Prediction Center Unified (CPCU) product  
101 (Xie et al. 2007). The L4 product provides global, 9-km, 3-hourly surface (0–5 cm) and root-zone (0–100 cm) soil  
102 moisture estimates along with related land surface fields and analysis diagnostics. For the present study, we aggregated  
103 all soil moisture estimates to daily-average (00:00 to 23:59 UTC) data. A baseline, model-only, ensemble CLSM  
104 simulation without the assimilation of SMAP Tb observations (but using the same perturbations as in the L4 system)  
105 is referred to as the “open-loop” (OL) run.

106 The SMAP L4 assimilation system includes a zero-order “tau-omega” forward RTM (De Lannoy et al., 2013) that  
107 converts SSM and surface soil temperature into L-band brightness temperature estimates. Selected parameters of the  
108 L4 RTM, including microwave soil roughness parameters, a vegetation structure parameter, and the microwave  
109 scattering albedo, were calibrated using multi-angular L-band brightness temperature observations from the Soil  
110 Moisture Ocean Salinity (SMOS) mission (De Lannoy et al., 2014). The L4 RTM parameterizes microwave soil  
111 roughness as a function of SSM (De Lannoy et al., 2013, their equation B1). Here, we used this parameterization to  
112 compute the 2017–2018 time-averaged microwave soil roughness estimates as one potential indicator of DA efficiency  
113 (Section 2.3). The necessary parameters were obtained from L4 “Land-Model-Constants” output Collection (last  
114 access: 8 July 2020; DOI: <https://doi.org/10.5067/KGLC3UH4TMAQ>; Reichle et al., 2018a). The L4 “Analysis-  
115 Update-Data” output Collection includes RTM predictions of Tb and the assimilated SMAP Tb observations (last  
116 access: 8 July 2020; DOI: <https://doi.org/10.5067/60HB8VIP2T8W>; Reichle et al., 2018b).



117 To avoid the impact of seasonality, we performed our analysis using anomaly time series, derived by subtracting a  
118 seasonally-varying (daily) climatology from each raw time series. The climatology of a given time series was obtained  
119 by sampling the mean value of all soil moisture estimates that fall within a 31-day moving window centered on a  
120 particular day-of-year. Moreover, L4 estimates of land latent heat flux (LE), land sensible heat flux (SH) and the  
121 climatological LAI inputs to CLSM and the RTM, were obtained from the L4 “Geophysical-Data” output Collection  
122 (last access: 6 April 2020; DOI: <https://doi.org/10.5067/KPJNN2G11DQR>; Reichle et al., 2018c). These datasets were  
123 also used to compute control factors to explain spatial variations in the DA efficiency of the L4 system (Section 2.3).

## 124 2.2 Soil moisture validation data

125 **In-situ soil moisture measurements during 2017 and 2018 were collected from a national network of Chinese**  
126 **Automatic Soil Moisture Observation Stations (CASMOS) maintained by the Chinese Meteorological Administration**  
127 **(CMA).** In total, soil moisture measurements from 2474 separate stations arrayed across mainland China, and covering  
128 different land use types, were collected. At each CASMOS site, frequency domain reflectometry-based instruments  
129 were used to record hourly volumetric soil moisture content within the following vertical depth ranges: 0–10, 10–20,  
130 20–30, 30–40, and 40–50 cm below the surface. These hourly estimates (at multiple depths) were then aggregated into  
131 daily values and linearly averaged (vertically) to produce 0-10 cm (SSM) and 0-50 cm (RZSM) in situ soil moisture  
132 measurements – which were subsequently used to validate the L4 and OL SSM (0-5 cm) and RZSM (0-100 cm)  
133 estimates. Note that Spearman correlation rather than Pearson correlation is used for L4 and OL validation, in order to  
134 avoid impact of outliers in the time series and prior assumptions about soil moisture distributions.


135 Ground observations falling within the same 9-km EASE grid were averaged for comparisons against the collocated  
136 9-km L4 and OL soil moisture estimates. A total of 2287 individual 9-km EASE grid cells within mainland China are  
137 included in the analysis. Among them, 92.35% of grid cells contain one in-situ site, 7.26% contain two sites, 7 grid  
138 cells contain three sites, and the remaining two grid cells contain four and five sites respectively.


## 139 2.3 Explanatory data products


140 As discussed above, our hypothesis is that the efficiency of the SMAP system will be sensitive to the ability of the  
141 ensemble-based L4 analysis in filtering errors that exist in the OL (that is, CLSM), in the model forecast Tb (that is,  
142 the RTM), and in the SMAP Tb observations. We therefore considered two separate categories of factors that  
143 potentially control spatial variations in DA efficiency. The factors are summarized in Table 1.


144 The first category represents a range of factors known to affect the skill of soil moisture estimates derived from LSM  
145 (in this case, CLSM). The five control factors in this category are: i) the error in precipitation forcing, ii) the error in  
146 (input) LAI, iii) the error in (output) LE, iv) the magnitude of mean error in CLSM SSM-RZSM coupling strength,  
147 and v) the presence of vertical variability in soil properties (defined as the difference in clay fraction across the vertical  
148 soil profile). Note that such variability represents a potential source of error because CLSM assumes that soil texture  
149 and the associated soil parameters are vertically homogeneous within the soil column, with the exception of some



150 surface-layer moisture transport parameters. The soil texture information is from Harmonized World Soil Database  
151 (HWSD) v1.2. 

152 The second category contains three factors that affect radiative transfer modeling (RTM) and therefore DA updates.  
153 These include: i) estimates of the joint error in SMAP Tb observations and RTM Tb simulations, ii) the magnitude of  
154 microwave soil roughness, and iii) the magnitude of LAI (as a proxy for the vegetation optical depth at microwave  
155 frequencies, which modulates the sensitivity of the observed Tb to SSM conditions). 

156 The control factors take a variety of forms. Some factors are based on estimates of the errors fed into the L4 system as  
157 (e.g., the error in CLSM rainfall forcing data). Other factors consist of the magnitude of the variable itself (e.g., the  
158 vertical variability of clay fraction). Note that LAI is used in both ways: LAI error is used to predict OL performance  
159 (because LAI is an important input into CLSM) while mean LAI is used to explain DA performance (because increased  
160 LAI is associated with decreased soil moisture information content in microwave observations). 

161 Note that the LAI used in the L4 system is a climatology derived from satellite observations of the Normalized  
162 Difference Vegetation Index. Therefore, to indicate the magnitude by which each grid cell's LAI typically deviates  
163 from its long-term climatology, we use the temporal standard deviation of anomaly time series of the benchmark LAI  
164 (from SPOT VGT product) as a measure of the error in the LAI used in L4. Owing to the lack of reference Tb  
165 observations at similar satellite overpass times and locations, Tb errors are gauged using the time series standard  
166 deviation of the observation-minus-forecast (O-F) Tb residuals, which indicate the typical misfit between the model  
167 forecast Tb and the rescaled SMAP Tb observations. This metric measures the total error in Tb observation space. 

168 The exact data sets and the metrics utilized for evaluating these 8 control factors are summarized in Table 1.



**Table 1** Benchmark data sets and metrics used for evaluating control factors of SMAP L4

Factor category	Control factor	Dataset/Benchmark	Temporal resolution	Spatial resolution	Data range	Metrics
	Precipitation error	Rain gauge (CGDPR17)	daily	0.25 °	2017-2018	Spearman's rank correlation <i>R</i>
	SSM-RZSM coupling strength error	CASMOS	daily	NA	2017-2018	ΔCP (see Section 2.4)
LSM	Vertical variability of clay fraction	HWSD	NA	9 km	NA	Difference in clay fraction between topsoil (0-30 cm) and root-zone (0-100 cm) layers
	SMAP L4 LAI error	SPOT LAI	10 d	1 km	2017-2018	Temporal standard deviation of SPOT VGT LAI anomaly
	LE error	FLUXCOM	daily	(1/120) °	2017-2018	IVd-based <i>R</i>
	Tb error	SMAP L4	daily	9 km	2017-2018	Temporal standard deviation of O-F Tb residuals
RTM	Microwave soil roughness	SMAP L4	daily	9 km	2017-2018	Temporal average based on De Lannoy et al. (2013)
	Annual mean LAI	MODIS/Geoland-based product	daily	9 km	2017-2018	Climatological mean



171 **2.3.1 Gauge-based precipitation gridded product**

172 Errors in the GEOS precipitation data used to force the CLSM within the SMAP L4 system were estimated via  
173 Spearman's rank correlation with available rain-gauge observations. These network observations are based on an  
174 analysis of ~2400 rain gauge stations distributed unevenly over mainland China. Recently, the China Gauge-based  
175 Daily Precipitation Analysis (CGDPA) with a spatial resolution of  $0.25^\circ \times 0.25^\circ$  based on this network was constructed  
176 and has been made operational over mainland China. CGDPA uses a modified interpolation method of climatology-  
177 based optimal interpolation (OI) with topographic correction proposed by Xie et al. (2007). In this process, daily  
178 precipitation climatology over mainland China is optimized and is rebuilt using the 30-year average precipitation  
179 observations from ~2400 gauges of the period 1971–2000 (Shen et al., 2010). CGDPA is shown to have smaller bias  
180 and root mean square error than the CPCU product used in L4, which is based on fewer than 400 gauge sites over  
181 mainland China (Shen et al., 2015).

182 **2.3.2 FLUXCOM LE estimates**

183 The FLUXCOM ensemble of global land-atmosphere energy fluxes was used to evaluate the error of the L4 LE  
184 estimates. This ensemble merges energy flux measurements from FLUXNET eddy covariance towers with remote  
185 sensing and meteorological data based on a machine learning method to estimate global gridded net radiation, latent  
186 and sensible heat and their related uncertainties (Jung et al., 2019). The resulting FLUXCOM database has a  $0.0833^\circ$   
187 spatial resolution when applied using MODIS remote sensing data. The monthly energy flux data of all ensemble  
188 members, as well as the ensemble estimates from the FLUXCOM initiative, are freely available (CC4.0 BY license)  
189 from the Data Portal (<http://fluxcom.org/>), while the daily- and 8-day FLUXCOM products are available upon request  
190 from dataset provider Martin Jung. To calculate the LE error, we've collected the daily, high spatial resolution  
191 FLUXCOM product and extracted the estimates where in-situ soil moisture sites located.

192 **2.3.3 SPOT VGT LAI**

193 The data set used as a benchmark for assessing leaf area index (LAI) errors present in the SMAP L4 analysis was  
194 derived from **SPOT/VEGETATION and PROBA-V LAI** products (version 2) that are generated every 10 days at  
195 spatial resolution of 1 km. The SPOT LAI version 2 product capitalizes on the development and validation of already  
196 existing products: CYCLOPES version 3.1 and MODIS collection 5 and the use of neural networks (Baret et al., 2013;  
197 Verger et al., 2008). The version 2 products are derived from top of canopy daily (S1-TOC) reflectances instead of  
198 normalized top of canopy 30-day composited reflectances as in the version 1. Compared to version 1, the compositing  
199 step is performed at the biophysical variable level instead of reflectance level. This ensures reduced sensitivity to  
200 missing observations and avoids the need for a BRDF model.

201 **2.3.4 HWSO soil texture**

202 The HWSO attribute database (v1.2) is a 30 arc-second raster database with 15773 different soil-mapping units. It  
203 provides information on the standardized soil parameters for topsoil (0–30cm) and subsoil (30–100 cm) separately. In





204 this study, we use the difference of clay fractions between topsoil (0-30cm) and the aggregated 0-100cm layer to  
205 measure the vertical clay fraction variation at each 9-km grid cell.

#### 206 **2.4 Vertical coupling metric**

207 The RZSM time series generally show decreased temporal dynamics relative to SSM. As a result, overestimated SSM-  
208 RZSM coupling tends to spuriously increase the (correlation-based) similarity of SSM and RZSM time series, and  
209 thereby, overestimate RZSM temporal variability. Therefore, analogous to Kling-Gupta efficiency (Gupta et al., 2009),  
210 we defined the SSM-RZSM coupling strength (CP) as:

$$CP = 1 - \sqrt{(R-1)^2 + (\alpha-1)^2} \quad (1)$$

211 where  $R$  is the Spearman's rank correlation between SSM and RZSM, and  $\alpha$  is the ratio of temporal standard deviation  
212 of SSM to that of RZSM. A CP value of one represents the extreme case where RZSM is identical to SSM, i.e., a  
213 strongly coupled case. Likewise, a CP of zero represents the opposing case of completely uncoupled time series. Cases  
214 with negative CP do not exist.

215 Observed CP ( $CP_{obs}$ ) was based on comparisons between 0-10 cm "surface" estimates and 0-50 cm "root-zone" in situ  
216 observations and used as a benchmark. In contrast, SMAP L4 CP estimates ( $CP_{OL}$ ) were based on the comparison of 0-  
217 5 cm "surface" estimates and 0-100 cm "root-zone" estimates. Therefore, the surface versus root-zone storage contrast  
218 in the observation time series is less than that of the L4 estimates. This will likely cause the observed correlation  
219 between surface and root-zone time series to be systematically higher than the analogous vertical correlation  
220 calculation for L4 estimates. However, this bias is partially corrected for by the second term in Eq. (1) – since the  
221 observed  $\alpha$  ratio will, by the same token, tend to be smaller (i.e. closer to one) than  $\alpha$  sampled from the L4 analysis.  
222 Such ability to compensate for vertical depth differences is a key reason we apply CP, rather than *simple correlation*,  
223 as a vertical coupling strength metric. Nevertheless, it should be noted that our main interest here lies in describing  
224 spatial variations in ( $CP_{OL} - CP_{obs}$ ) and care should be taken when interpreting raw ( $CP_{OL} - CP_{obs}$ ) differences as an  
225 *absolute* measure of L4 vertical coupling bias.

#### 226 **2.5 Double instrumental variable (IVd) method**

227 The benchmark data set of FLUXCOM LE described above contains error that is (likely) similar order of  
228 magnitude as the L4 LE dataset it is applied to evaluate. Therefore, in an attempt to correct for the impact of this error,  
229 the LE error used here as a control factor is obtained via a double instrumental variable (IVd; Dong et al., 2019b)  
230 analysis approach that minimizes the spurious impact of random errors in benchmark data sets. As shown in Dong et  
231 al. (2019b), for the evaluation of two time series with auto-correlation in both of them, IVd is more robust than single  
232 instrumental variable based algorithm, therefore we apply IVd to evaluate the LE error.



233 IVd is a modified version of triple collocation (TC) analysis. In TC analysis (McColl et al., 2014), geophysical  
234 variables obtained from three independent sources ( $x$ ,  $y$  and  $z$ ) are assumed to be linearly related to the true signal  $P$   
235 as:

$$x = \alpha_x P + B_x + \varepsilon_x \quad (2)$$

236 where the  $\alpha_x$  is a scaling factor;  $B_x$  is a temporal constant bias and  $\varepsilon_x$  is zero-mean random error.

237 As opposed to the TC method, IVd uses only two independent products ( $x$ ,  $y$ ) to characterize geophysical data product  
238 errors. This method introduces two instrumental variables ( $I$  and  $J$ , i.e.,  $I_t = \alpha_x P_{t-1} + B_x + \varepsilon_{xt-1}$ ,  $J_t = \alpha_y P_{t-1} + B_y + \varepsilon_{yt-1}$ ),  
239 which are based on the lag-1 (day) time series (at day  $t$ ) of  $x$  and  $y$ , respectively. Therefore, assuming that the errors of  
240 two independent products are serially white, the covariance between instrumental variables and products can be written  
241 as follows:

$$C_{Ix} = \alpha_x^2 L_{PP} \quad (3)$$

$$C_{Jy} = \alpha_y^2 L_{PP} \quad (4)$$

242 where  $C$  represents the covariance of the subscript products. For instance,  $C_{Ix}$  represents the covariance of  $x$  and its  
243 instrumental variable  $I$ . Variable  $L_{PP}$  is the lag-1 auto-covariance of the true signal. Combining Eqs. (3) and (4), the  
244 scaling ratio  $s_{ivd}$  of the two products  $x$  and  $y$  can be written as:

$$s_{ivd} = \sqrt{\frac{C_{Ix}}{C_{Jy}}} \quad (5)$$

245 Based on Eq. (5), their correlation with truth can be estimated as:

$$R_{Px}^2 = \frac{C_{xy} s_{ivd}}{C_{xx}} \quad (6)$$

$$R_{Py}^2 = \frac{C_{xy}}{C_{yy} s_{ivd}} \quad (7)$$

246 In this way, the error in the L4 LE (measured by IVd-based correlation with truth) can be estimated robustly using the  
247 FLUXCOM LE product described in Section 2.3.2.





## 248 2.6 Random forest regression

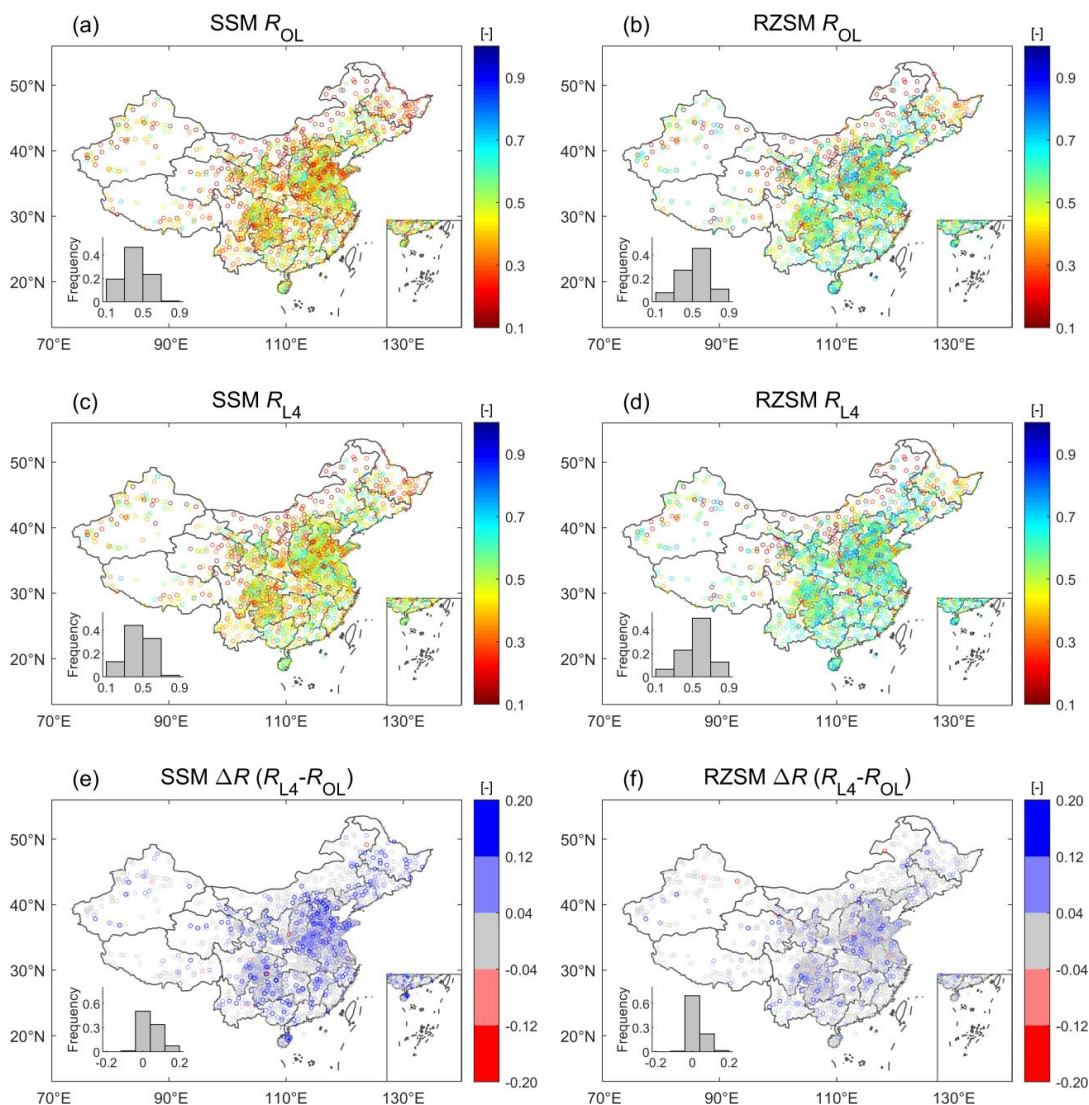
249 A random forest (RF) regression approach was used to rank and quantify the importance of the 8 control factors  
250 introduced above (Table 1) for describing spatial patterns in DA efficiency for both SSM and RZSM estimates. The  
251 RF method is a supervised learning algorithm based on an averaged ensemble of decision trees (Breiman, 2001). Unlike  
252 linear regression approaches, RF can capture non-linear interactions between the features and the target. In addition,  
253 the normalization (or scaling) of data is not necessary in RF application. Another advantage of the RF algorithm is that  
254 it can readily measure the relative importance of each feature on the estimates, which makes it highly suitable for an  
255 attribution analysis. Therefore, based on the output of RF, key control factors determining the efficiency of SMAP  
256 DA were evaluated and ranked. The RF estimates are based on a 10-fold cross-validation approach.

## 257 3 Results

### 258 3.1 Validation of SMAP L4 and OL estimates of SSM and RZSM anomalies

259 Figure 1 maps validation results (i.e., anomaly Spearman's rank correlation with in-situ observations,  $R$ ) for SMAP L4  
260 and associated OL soil moisture estimates. The skill patterns for OL and L4 are, in general, quite spatially consistent  
261 **Both are characterized by an increasing trend of SSM estimation skill moving from northwest to southeast China**   
262 1a and 1b). In relative terms, the L4 product surpasses the baseline OL's SSM skill within 77% of the 2287 9-km  
263 EASE grid cells containing ground observations – with a mean  $R$  increase of  $\Delta R = 0.056$  [-] and mean relative  
264 improvement versus  $R_{OL}$  of 14%.

265 Similar spatial patterns are observed for RZSM skill. As with SSM, generally higher consistency with in-situ RZSM  
266 measurements is found in southeast China relative to northern China. However, relative to SSM, the added value of  
267 SMAP data assimilation (i.e. L4) is reduced for RZSM and the mean relative  $R$  improvement falls to 7% ( $\Delta R = 0.034$   
268 [-]) (compare Fig. 1e and 1f). This is **not surprising**  assimilated SMAP Tbs are primarily sensitive to soil moisture  
269 conditions in the surface (0-5 cm) layer.



270

271 **Figure 1: OL (a, b) and L4 (c, d) skills ( $R$  values) for SSM (left column) and RZSM (right column). DA efficiency ( $\Delta R = R_{L4}$**   
 272 **-  $R_{OL}$ ) for (e) SSM and (f) RZSM. Blue (red) colors in (e) and (f) indicate grid cells where L4 estimates are better (worse)**  
 273 **than OL. Non-significant differences (based on a 1000-member bootstrapping analysis) are colored grey. The lower left inset**  
 274 **in each subplot indicates the frequency of binned  $R$ -values across all 9-km EASE grid cells containing ground observations.**

275

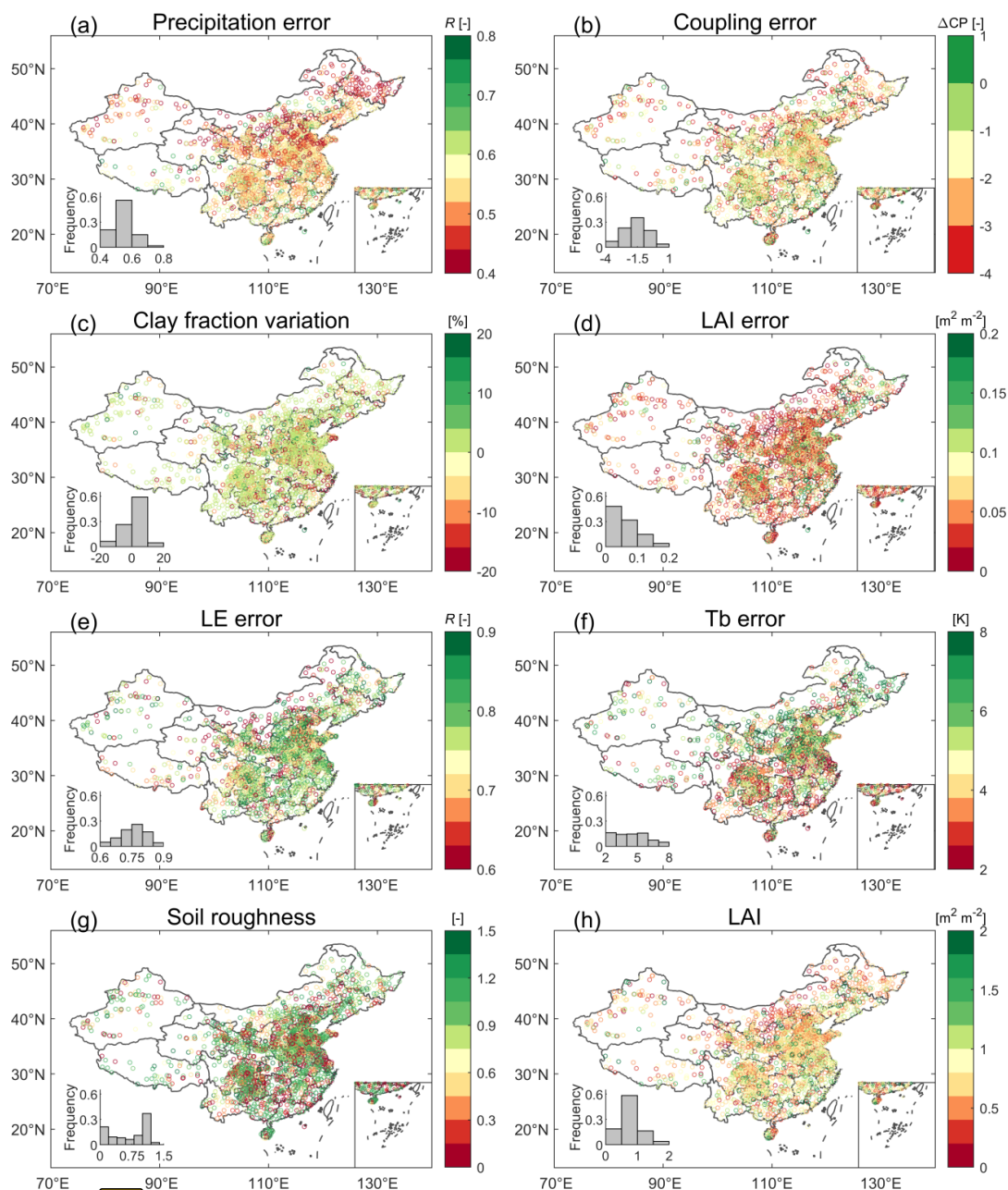
### 276 3.2 Spatial distribution of potential factors controlling SMAP L4 DA performance

277 As described in Section 2.3, we selected 8 control factors that potentially influence the skill of SMAP L4 soil moisture  
 278 estimates. Using the attribution analysis described in Section 2.6, these factors will be used to explain the spatial



279 variations in skill and DA efficiency seen in Fig. 1. As a first step, this section examines the spatial patterns inherent  
280 in the 8 control factors. Errors in the CLSM precipitation forcing are relatively higher in northern and northwestern  
281 areas of China (Fig. 2a), where the gauge density is generally more sparse than southern China. Among the factors  
282 representing CLSM structural errors, a pre-dominantly negative bias is observed in SSM-RZSM coupling strength  
283 generally across China (i.e., lower  $CP_{OL}$  compared to  $CP_{obs}$ ), while a very small number of grid cells show a positive  
284 coupling strength bias in eastern China (dark green dots in Fig. 2b). This is expected since at the coarse resolution, the  
285 model's vertical coupling strength **should be much less than** a single point. In addition, this may be partly  
286 attributed to the layer depths differences, since CLSM represents surface and root-zone depths of 0-5 cm and 0-100  
287 cm, whereas the corresponding in-situ observations represent the 0-10 cm and 0-50 cm layers, and it can be expected  
288 that  $CP_{OL}$  **should** thus be smaller than  $CP_{obs}$ . In addition, the vertical variability of the clay fraction seems to show little  
289 spatial variation across mainland China (Fig. 2c). With respect to CLSM LAI error, regions in southern China that  
290 have generally higher LAI show larger standard deviation in SPOT LAI time series (Fig. 2d and 2h). The IVd-based  
291 estimates of SMAP L4 LE error, which represent a potential control factor for water-balance errors in CLSM, generally  
292 show low-level of error across mainland China (Fig. 2e).

293 For O-F Tb residuals describing RTM-related error, a higher standard deviation of O-F Tb residuals is observed in the  
294 North China Plain (Fig. 2f), which is very consistent in spatial distribution with areas displaying the highest and most  
295 significant SSM prediction improvement (Fig. 1c). This is expected, as mentioned above, because O-F Tb residuals  
296 are the basis for the soil moisture corrections (or increments) that are applied in the DA system as part of the L4  
297 analysis. The 2017-2018 mean of soil roughness and the 2017-2018 mean LAI show higher values in southwest and  
298 southeast China (Fig. 2g-h).



299

**Figure 2:** Factors potentially influencing SMAP L4 performance over mainland China: (a) CLSM precipitation error measured by the Spearman's rank correlation between CLSM precipitation and ground observations; (b) SSM-RZSM coupling strength error ( $CP_{OL}$  minus  $CP_{obs}$ ); (c) clay fraction variation (difference) across the soil profile; (d) error in LAI input to L4; (e) IVD-based error of LE from L4; (f) Tb error; (g) L4 microwave soil roughness; (h) climatology mean of LAI input to L4.

300  
 301  
 302  
 303  
 304



305

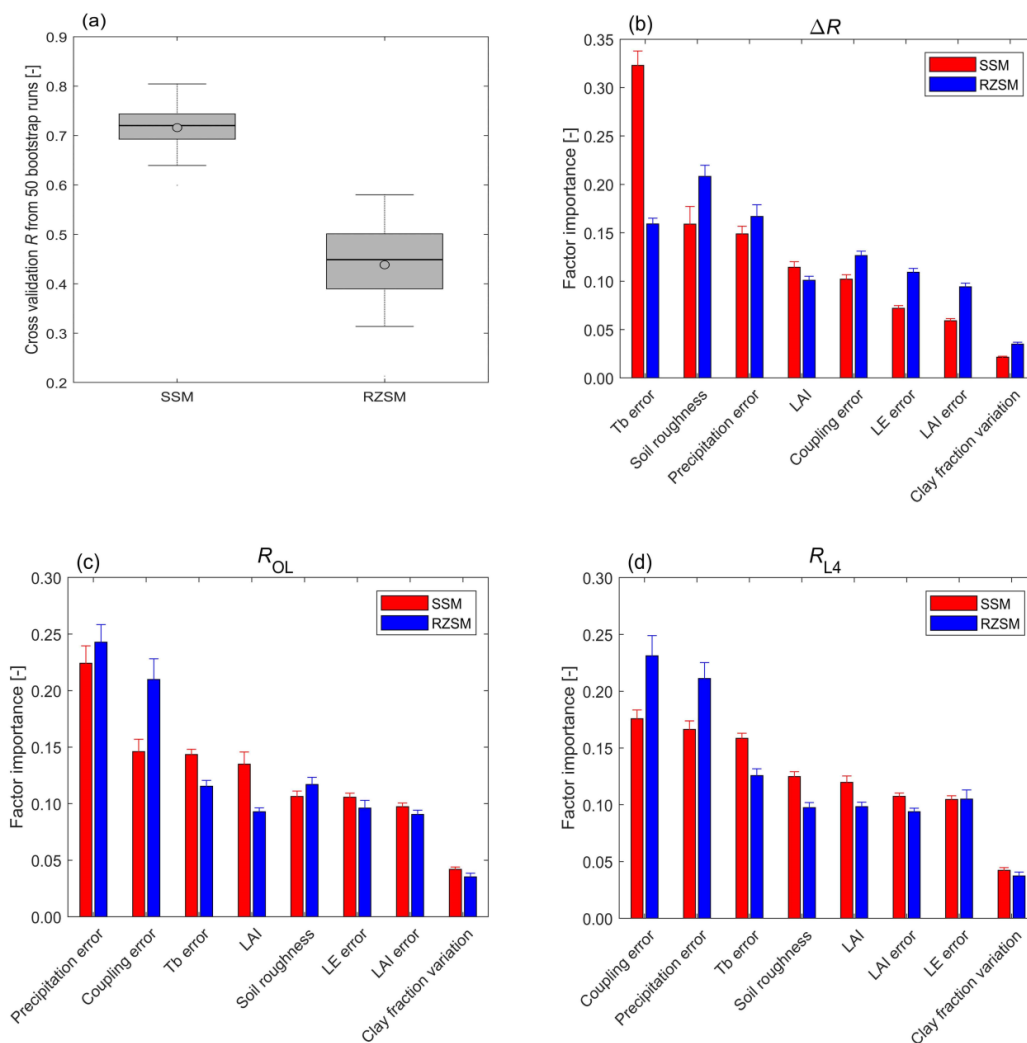
### 306 3.3 Attribution of SMAP L4 versus OL performance to control factors

#### 307 3.3.1 Attribution using random forest regression

308 As mentioned above, RF regression was used to identify the relative importance of our 8 control factors for determining  
309 the efficiency of SMAP L4 DA (i.e.,  $\Delta R = R_{L4} - R_{OL}$ ) also L4 ( $R_{L4}$ ) and OL performances ( $R_{OL}$ ). To start, we first  
310 investigate the robustness of RF for predicting  $\Delta R$ . To estimate the magnitude of randomness in the RF algorithm, we  
311 use 50 bootstrap runs. As shown in Fig. 3a, the 10-fold cross-validation test (228 validation samples) shows that the  
312 predicted and in-situ-based  $\Delta R$  have a mean correlation of 0.72 and 0.46 for SSM and RZSM, respectively.

313 Given the sampling errors of  $\Delta R$ , which is based on a two-year validation period, and the relatively low spatial  
314 variability in RZSM skill (Figs. 1f), the performance of RF is acceptable. In addition, ground-measurement upscaling  
315 error is likely a significant contributor to unexplainable spatial variability for  $\Delta R$  in Fig. 1. In fact, Chen et al. (2016)  
316 found large spatial variability in the ability of point-scale SSM ground observations to describe grid cell-scale SSM  
317 dynamics. In-situ observations sites associated with larger upscaling errors introduce a spurious low bias into  
318 sampled estimates of  $\Delta R$  values (see Appendix B in Dong et al., 2020). Therefore, some of the  $\Delta R$  spatial variability  
319 observed in Fig. 1 is unrelated to any aspect of the L4 system and is therefore unexplainable via the 8 control factors  
320 we have selected.

321



322

323 **Figure 3.** Distribution analysis of SMAP L4 DA efficiency: (a) Cross-validation of RF regression method in predicting DA  
 324 efficiency  $\Delta R = R_{L4} - R_{OL}$  based on our 8 control factors (Table 1). Relative importance of 8 control factors determining  
 325 spatial patterns in (b) DA efficiency ( $\Delta R$ ), (c) OL performance ( $R_{OL}$ ), and (d) L4 performance ( $R_{L4}$ ). Red (blue) bars  
 326 represent predictor importance for SSM (RZSM). Error bars reflect the standard deviation from 50-member bootstrapping  
 327 of the RF importance estimates.

328

329 Based on the RF results, the Tb error is quantified as the most prominent factor in determining DA efficiency (i.e.,  $\Delta R$   
 330 =  $R_{L4} - R_{OL}$ ) – followed by precipitation error and microwave soil roughness (Fig. 3b). The RF-derived ranking of  
 331 control-factor importance for RZSM is similar to that of SSM in that the same three factors are still the most





332 explanatory. However, in contrast to SSM, the importance of Tb error for RZSM decreased dramatically from >30%  
333 to ~15%. Other modeling error sources (e.g., the vertical variability of soil properties) have only very limited impact  
334 on SMAP DA improvement.

335 As seen in Fig. 3c, for the OL performance ( $R_{OL}$ ) the most important factors identified by RF include precipitation  
336 error, SSM-RZSM coupling error, and Tb error (microwave soil roughness) for SSM (RZSM). Note that although the  
337 Tb error is identified as third important factor for  $R_{OL}$  in SSM skill, this is an instance where there is correlation (poorer  
338 skill happens to coincide with higher Tb error), but this does not imply a causal relationship. Specifically, it is normal  
339 that Tb (O-F) errors are higher where the OL performs worse, but a high Tb error is not the cause of a low OL  
340 performance. The same applies to the relationship between microwave soil roughness and OL skill for RZSM  
341 estimation. The SMAP L4 system is able to reduce the predominant impact of precipitation errors on both SSM and  
342 RZSM estimation skill, rendering SSM-RZSM coupling error the most important factor for  $R_{L4}$  (Fig. 3d). In addition,  
343 in the L4 system, the high vegetation density effect on SSM and RZSM estimation is clearly reduced, as the fourth  
344 most important factor of LAI is replaced by Tb error.

345 The qualitative rankings provided by the RF analysis in Fig. 3 are relatively robust to our particular choice of  
346 benchmark data set to define the ‘error’ of various control variables. For instance, we replaced the CGDPA  
347 precipitation benchmark with the CMORPH-merge product (Version 1, last access: 6 April 2020; DOI:  
348 <https://doi.org/10.25921/w9va-q159>; Xie et al., 2019), which is the 0.1 degree merging product of CMORPH and  
349 observations from more than 30,000 automatic weather stations in mainland China. For this case, the predictive power  
350 of the regression model established by the RF is not affected (similar to Fig. 3a), and the qualitative rankings of the  
351 precipitation error in  $R_{OL}$  and  $R_{L4}$  are not impacted (similar to Fig. 3c-d).

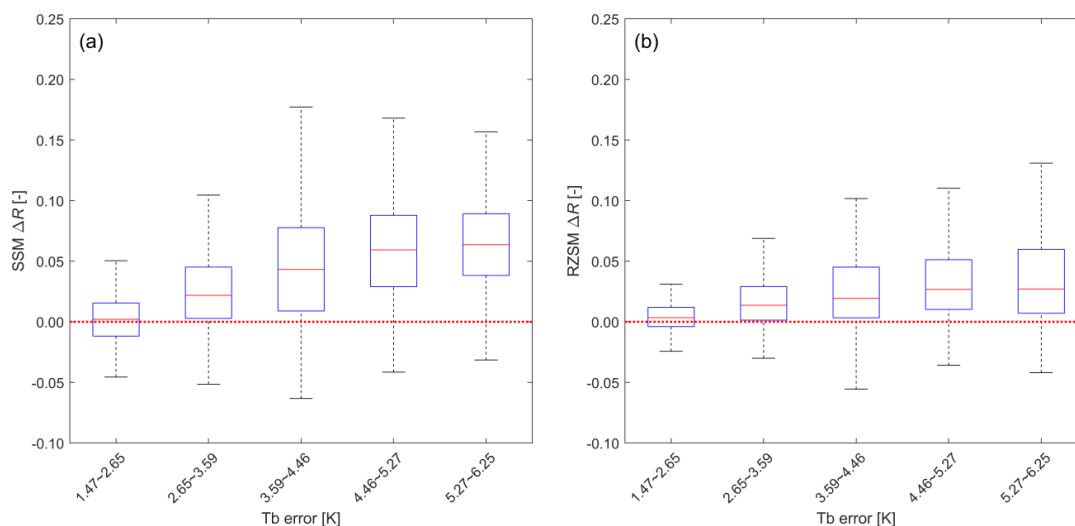
352

### 353 3.3.2 Attribution using box plot comparisons

354 As stated in Section 2.5, the RF method is adept at summarizing the impact of multiple (co-varying) control factors  
355 simultaneously in the established regression model and thus provides more comprehensive insights than the  
356 examination of how the target variable (DA improvement) fluctuates with each individual control factor. However, it  
357 does not allow the investigation of the sign of the relationship between DA improvement and each control factor –  
358 which is important for understanding exactly how each factor influences the DA system. In addition, since the net  
359 impact of various factors can enhance DA efficiency by either degrading the OL or enhancing the ability of DA to add  
360 more value, it is important to decompose the source of variations in  $\Delta R$ . Therefore, in addition to examining how  
361 SMAP DA efficiency, i.e.,  $\Delta R = R_{L4} - R_{OL}$ , varies as a function of the most prominent control factors identified in the  
362 above Section 3.3.1 (i.e., Tb error, precipitation forcing, and microwave soil roughness), we also examine how  
363 precipitation error as a control factor affects the OL performance, i.e.,  $R_{OL}$ .



364 To minimize the uncertainty caused by large errors in each of the control factors, we exclude samples with errors  
365 (separately for each control factor) ranking above the 80th percentile in the following analysis. The relationship  
366 between Tb errors and L4 DA efficiency is straightforward: higher Tb errors are associated with higher  $\Delta R$ , with  $\Delta R$   
367 generally larger for SSM than for RZSM (Fig. 4a-b).

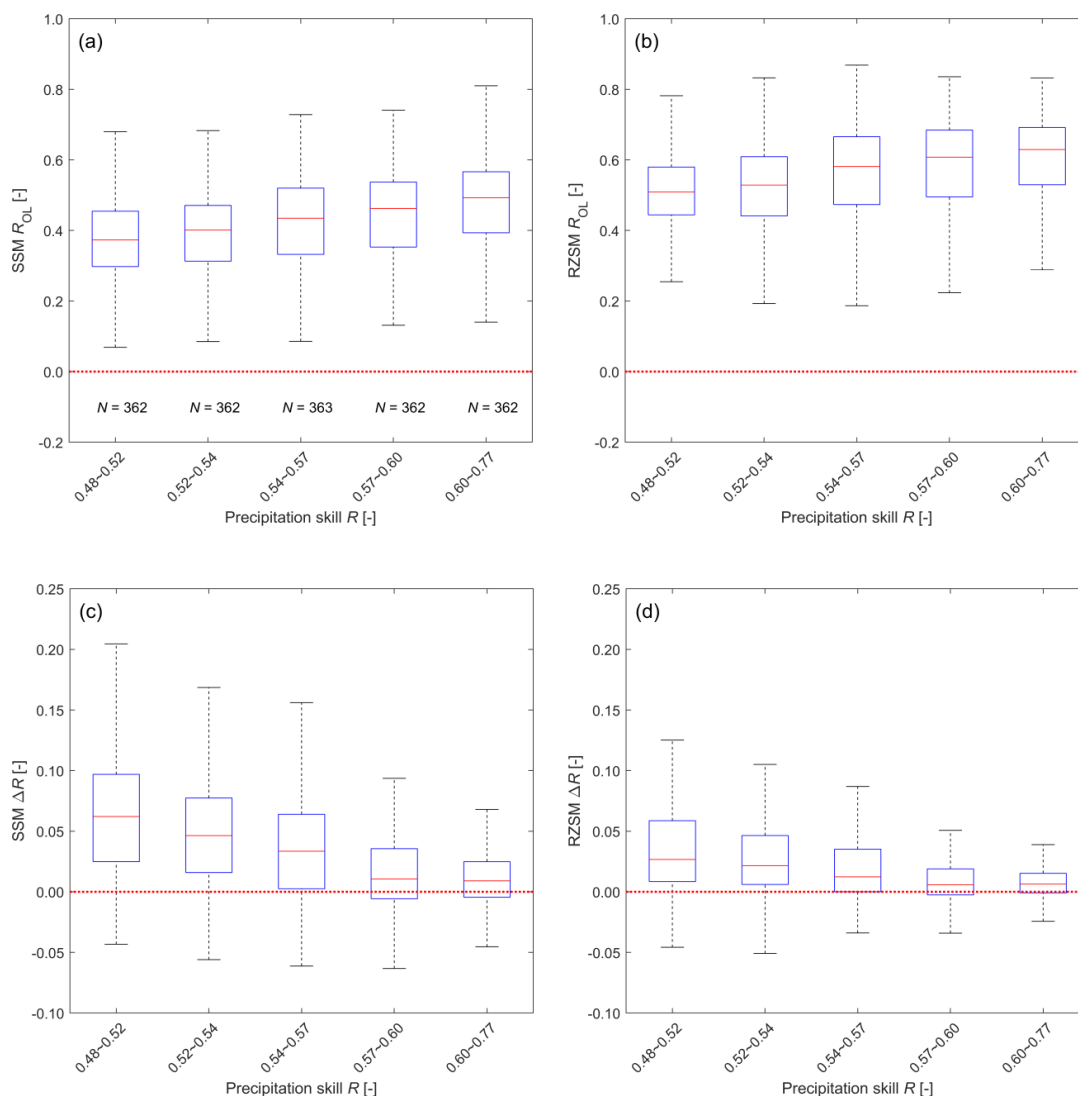


368

369 **Figure 4: SMAP L4 DA efficiency ( $\Delta R = R_{L4} - R_{OL}$ ) as a function of Tb error for (a) SSM and (b) RZSM. Samples with Tb**  
370 **error ranking above the 80th percentile are excluded from the analysis.**

371

372 For precipitation, this decomposition is illustrated in Fig. 5. Note that, as expected, low-quality precipitation tends to  
373 degrade the skill (i.e., correlation versus ground observations) of OL SSM and RZSM estimates (see Fig. 5a-b). This  
374 degradation provides an enhanced opportunity for SMAP L4 DA to provide added value. As a result,  $\Delta R$  tends to be a  
375 proportional function of precipitation skill (i.e., higher precipitation skill leads to lower  $\Delta R$ , see Fig. 5c-d). This inverse  
376 relationship is a well-known tendency for land data assimilation systems (Liu et al., 2011; Bolten and Crow, 2012;  
377 Dong et al., 2019a). Precipitation quality has a diminished impact on RZSM estimation skill compared to SSM  
378 estimation skill. This is expected since RZSM is (essentially) the result of applying a low-pass time series filter to  
379 precipitation. As such, it is less sensitive to high-frequency errors in precipitation products than SSM is.



380

381

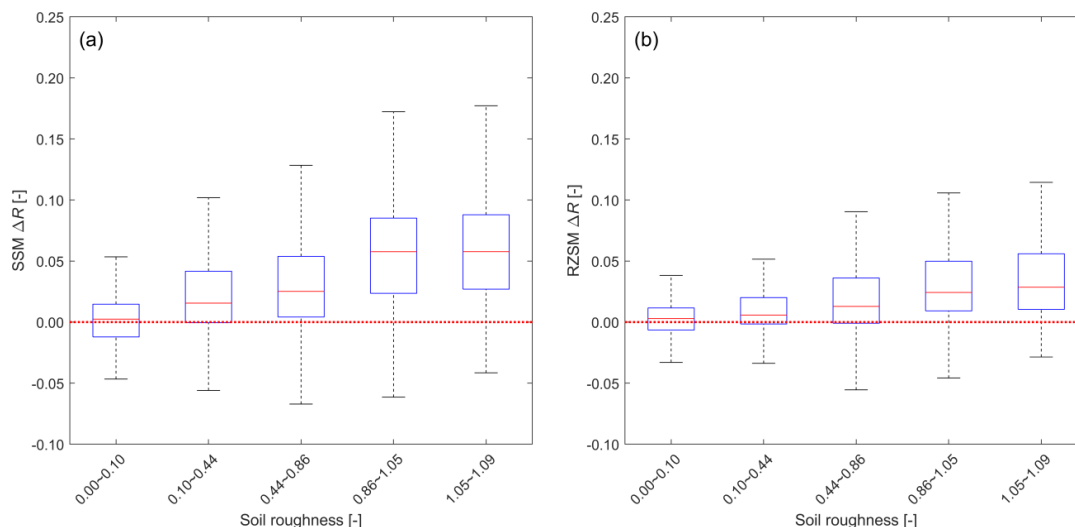
382 **Figure 5: OL performance ( $R_{OL}$ ) as a function of precipitation forcing skill  $R$  for (a) SSM and (b) RZSM. SMAP L4 DA**  
 383 **efficiency ( $\Delta R = R_{L4} - R_{OL}$ ) as a function of precipitation skill for (c) SSM and (d) RZSM. Samples with precipitation skill**  
 384 **ranking below the 20th percentile are excluded from the analysis.**

385

386 Figure 6 is analogous to Fig. 4 but shows skill differences  $\Delta R$  as a function of microwave soil roughness. Similar to  
 387 Tb errors, it is as expected that this control factor of microwave soil roughness has little impact on the OL performance,  
 388 except that  $R_{OL}$  shows slight decreasing tendency with increasing soil roughness (not shown). Given the fact that the



389 OL does get worse with increasing roughness, there is more room for improvement as the roughness increases, which  
390 makes it plausible that  $\Delta R$  increases with increasing soil roughness (see Fig. 6a-b).




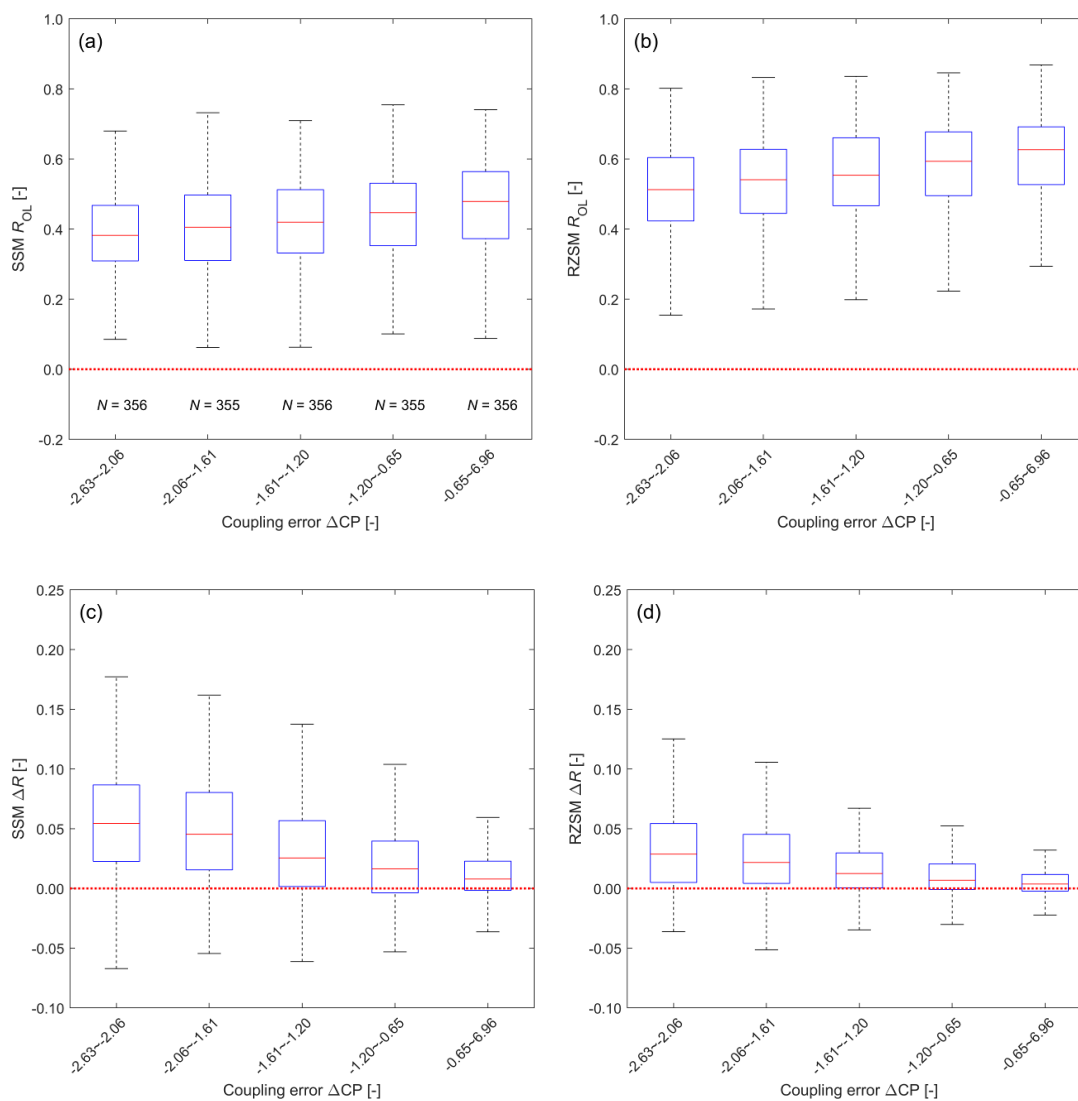
391

392 **Figure 6:** As in Fig. 4 but for  $\Delta R$  as a function of microwave soil roughness.

393

394 Besides the above three control factors that dominate the DA efficiency, we also examine the top factor that affects  
395 SMAP L4 performance, i.e., vertical-coupling errors (Fig. 7). As expected, larger (absolute) bias in SSM-RZSM  
396 coupling in CLSM tends to be associated with degraded OL estimates of both SSM and RZSM (see Figs. 7a-b),  
397 although the analysis does not prove such a causal relationship. Similar to precipitation errors above, decreased OL  
398 skill (seen on the left-hand-side of the figures) provides an opportunity for increased DA efficiency – which is clearly  
399 seen in Fig. 7. However, such increases are much larger for SSM than for RZSM.

400 For RZSM, SSM-RZSM coupling bias represents a **double-edged sword**  while such bias leads to an enhanced  
401 opportunity to improve upon a degraded OL, it should also hamper the ability of DA to transfer SSM increments into  
402 the root-zone – particularly when, like here, the bias reflects the lack of vertical coupling in the model (Kumar et al.,  
403 2009). This means that some of the opportunity presented by the larger OL RZSM errors is squandered by sub-optimal  
404 DA. As a result, the increase in RZSM DA efficiency associated with biased SSM-RZSM coupling (Fig. 7d) is smaller  
405 than the analogous increase in SSM DA efficiency (Fig. 7c).



406

407


408 **Figure 7:** As in Fig. 5 but for  $R_{OL}$  and  $\Delta R$  as a function of SSM-RZSM coupling error indicated by the CP difference ( $\Delta CP$   
 409 =  $CP_{OL} - CP_{obs}$ ).

410


411 For the three strongest control factors that determine DA efficiency  $\Delta R$ , i.e., Tb error, precipitation error and  
 412 microwave soil roughness, we further conducted paired one-way analysis of variance (not shown). Results indicates  
 413 that for each of the five binned groups separated by each of the above-mentioned three control factors, the inter-group  
 414 difference in  $\Delta R$  caused by each control factor is significant ( $p < 0.01$ ) for both SSM and RZSM. In addition, except for




415 the groups with lowest mean  $\Delta R$  in Fig. 4a and Fig. 6a, the averages of  $\Delta R$  from all groups are significantly higher  
416 than 0 ( $p < 0.01$ ).

417 As expected, precipitation error is the dominant factor for explaining the skill of the OL estimates. In contrast, the  
418 SSM-RZSM coupling error is the dominant factor for explaining the skill of the L4 results, which shows DA is able to  
419 correct for precipitation errors. 


#### 420 4 Conclusions

421 The SMAP L4 algorithm assimilates L-band Tb observations into the Catchment Land Surface Model, to provide  
422 surface and root-zone soil moisture estimates (i.e., SSM, RZSM) with global, 3-hourly coverage at 9-km resolution.  
423 The performance of the L4 soil moisture estimates compared to a baseline model-only simulation (OL) is influenced  
424 by multiple control factors associated with the land surface modelling (LSM) and radiative transfer modeling (RTM)  
425 components of the L4 system. In this study, we assess the performance of SMAP L4 DA system using the 2 years of  
426 in-situ soil moisture profile observations at 2474 sites across mainland China. We apply a random forest (RF)  
427 regression to identify the dominant factors  control the spatial distribution of the DA efficiency (defined as the skill  
428 difference between the L4 and OL estimates of SSM and RZSM as measured by their Spearman rank correlation with  
429 in-situ measurements). Results show that L4 improves SSM prediction skill by 14% on average, with over 77% of the  
430 2287 9-km EASE grid cells showing an increase in Spearman's rank correlation with in-situ observations. Similarly  
431 widespread but smaller improvements are also observed in RZSM, with averaged  $R$  improvement of 7%.

432 Based on the RF regression analysis, the added value of SMAP L4 DA for SSM is primarily determined by Tb error  
433 (measured by standard deviation of O-F Tb residuals), followed by microwave soil roughness and daily precipitation  
434 error. These three factors are also the most prominent factors controlling SMAP DA improvement for RZSM, albeit  
435 with the Tb error being the least important of these three factors for RZSM DA efficiency.

436 Generally, the OL performance clearly decreases with increasing precipitation error.  as for L4 performance  
437 precipitation error is not identified as the most dominant control factor. This indicates that the L4 system is able to  
438 correct for errors in precipitation forcing. In addition, our results demonstrate that SMAP DA contributes the most  
439 added value for cases where CLSM underestimates SSM-RZSM vertical coupling strength. However, due to the  
440 difference in top-layer soil depth between the in-situ observations (10 cm) and the L4 analysis (5 cm), it is unclear  
441 whether or not the observed SSM-RZSM coupling strength biases are real in an absolute sense – or simply reflect  
442 inconsistencies in the depth of modelled versus observed SSM and RZSM time series. Nevertheless, it is worth  
443 stressing that, despite the ambiguity with regards to their absolute magnitude/sign, relative variations in apparent SSM-  
444 RZSM coupling biases explain a significant amount of the observed spatial variation in L4 performance. Therefore,  
445 this finding clearly underpins the importance of properly specifying SSM-RZSM coupling strength in CLSM as a way  
446 to improve the SMAP L4 product.



447 For SMAP L4 SSM skill, the next-most important factors (after SSM-RZSM coupling) are the precipitation error, the  
448 Tb error and microwave soil roughness (Fig. 3d). For L4 RZSM skill, the next-most important factors (after SSM-  
449 RZSM coupling) are the precipitation error, the Tb error and the LE error, with the latter two factors of comparable  
450 importance (Fig. 3d). To enhance the L4 performance, additional focus should thus be placed on improving the model's  
451 characterization of the partitioning of the available energy into latent and sensible heat (LE error) and the microwave  
452 radiative transfer modeling (Tb error). 

#### 453 **Data availability**

454 The SMAP L4 datasets are available from <https://nsidc.org/data/SPL4SMAU/versions/4>. Gauge-based precipitation  
455 dataset CGDPA is from [http://data.cma.cn/data/cdcdetail/dataCode/SEVP\\_CLI\\_CHN\\_PRE\\_DAY\\_GRID\\_0.25.html](http://data.cma.cn/data/cdcdetail/dataCode/SEVP_CLI_CHN_PRE_DAY_GRID_0.25.html).  
456 The availabilities of other datasets are stated in their corresponding subsections.

#### 457 **Author contributions**

458 Jianxiu Qiu and Jianzhi Dong conceptualized the study. Jianxiu Qiu carried out the analysis and wrote the first draft  
459 manuscript, Wade Crow refined the work, Jianzhi Dong, Rolf Reichle, and Gabrielle De Lannoy helped with the analysis.  
460 All authors contributed to the analysis, interpretation of the results and writing.

#### 461 **Competing interests**

462 The authors declare that they have no conflict of interest.

#### 463 **Acknowledgments**

464 This work was supported by National Natural Science Foundation of China (Grant Nos. 41971031, 41501450). Rolf  
465 Reichle was supported by the NASA SMAP mission. Gabrielle De Lannoy was supported by KU Leuven C1  
466 (C14/16/045). The findings, conclusions and representations of fact in this publication are those of the authors and should  
467 not be construed to represent any official USDA or U.S. Government determination or policy.

#### 468 **References**

- 469 Baret, F., Weiss, M., Lacaze, R., Camacho, F., Makhmara, H., Pacholczyk, P., and Smets, B.: GEOV1: LAI, FAPAR  
470 Essential Climate Variables and FCOVER global time series capitalizing over existing products. Part1: Principles of  
471 development and production, *Remote Sens. Environ.*, 137, 299-309, doi:10.1016/j.rse.2013.02.030, 2013.  
472  
473 Bolten, J.D. and Crow, W.T.: Improved prediction of quasi-global vegetation conditions using remotely-sensed  
474 surface soil moisture, *Geophys. Res. Lett.*, 39(19), doi:10.1029/2012GL053470, 2012.



475  
476 Breiman, L.: Random forests, *Mach. Learn.*, 45(1), 5–32, doi:10.1023/A:1010933404324, 2001.  
477  
478 Chan, S., Njoku, E. G. and Colliander A.: SMAP L1C radiometer half-orbit 36 km EASE-Grid brightness temperatures,  
479 version 3. NASA National Snow and Ice Data Center Distributed Active Archive Center, 10.5067/E51BSP6V3KP7,  
480 2016.  
481  
482 Chen, F., Crow, W.T., Starks, P.J. and Moriasi, D.N.: Improving hydrologic predictions of a catchment model via  
483 assimilation of surface soil moisture, *Adv. Water Resources.*, 34(4), 526-536, doi:10.1016/j.advwatres.2011.01.011,  
484 2011.  
485  
486 Chen, F., Crow, W.T., Colliander, A., Cosh, M.H., Jackson, T.J., Bindlish, R., Reichle, R.H., Chan, S.K., Bosch, D.D.,  
487 Starks, P.J., and Goodrich, D.C.: Application of triple collocation in ground-based validation of Soil Moisture  
488 Active/Passive (SMAP) level 2 data products, *IEEE JSTARS.*, 99, 1-14, doi:10.1109/JSTARS.2016.2569998, 2016.  
489  
490 Crow, W.T. and Van Loon, E.: The impact of incorrect model error assumptions on the sequential assimilation of  
491 remotely sensed surface soil moisture, *J. Hydrometeorol.*, 8(3), 421-431, doi:10.1175/jhm499.1, 2006.  
492  
493 De Lannoy, G. J. M., Reichle, R. H., and Pauwels, V. R. N.: Global calibration of the GEOS-5 L-band microwave  
494 radiative transfer model over nonfrozen land using SMOS observations, *J. Hydrometeorol.*, 14(3), 765–785,  
495 doi:10.1175/JHM-D-12-092.1, 2013.  
496  
497 De Lannoy, G. J. M., Reichle, R. H., and Vrugt, J. A.: Uncertainty quantification of GEOS-5 L-band radiative transfer  
498 model parameters using Bayesian inference and SMOS observations, *Remote Sens. Environ.*, 148, 146–157,  
499 doi :10.1016/j.rse.2014.03.030, 2014.  
500  
501 Dong, J., Crow, W.T., Reichle, R., Liu, Q., Lei, F., and Cosh, M.: A global assessment of added value in the SMAP  
502 Level 4 soil moisture product relative to its baseline land surface model, *Geophys. Res. Lett.*, 46, 6604-6613,  
503 doi:10.1029/2019GL083398, 2019a.  
504  
505 Dong, J., Crow, W.T., Duan, Z., Wei, L., and Lu, Y.: A double instrumental variable method for geophysical product  
506 error estimation, *Remote Sens. Environ.*, 225, 217-228, doi:10.1016/j.rse.2019.03.003, 2019b.  
507  
508 Dong, J., Crow, W.T., Tobin, J. K., Cosh, H. M., Bosch, D. D., Starks, J. P., Seyfried, M., and Collins, H. C.:  
509 Comparison of microwave remote sensing and land surface modeling in surface soil moisture climatology estimation,  
510 *Remote Sens. Environ.*, 242, 111756, doi :10.1016/j.rse.2020.111756, 2020.  
511





- 512 Entekhabi, D., Njoku, E. G., O'Neill, P. E., Kellogg, K. H., Crow, W. T., and Edelstein, W. N.: The soil moisture active  
513 passive (SMAP) mission, *P. IEEE.*, 98(5), 704–716, doi:10.1109/jproc.2010.2043918, 2010.
- 514
- 515 Gruber, A., De Lannoy, G., Albergel, C., Al-Yaari, A., Brocca, L., Calvet, J. C., and Draper, C.: Validation practices  
516 for satellite soil moisture retrievals: What are (the) errors?, *Remote Sens. Environ.*, 244, 111806,  
517 doi:10.1016/j.rse.2020.111806, 2020.
- 518
- 519 Gupta, H. V., Kling, H., Yilmaz, K. K., and Martinez, G. F.: Decomposition of the mean squared error and NSE  
520 performance criteria: Implications for improving hydrological modelling, *J. Hydrometeorol.*, 377(1-2), 80-91,  
521 doi:10.1016/j.jhydrol.2009.08.003, 2009.
- 522
- 523 Jung, M., Koirala, S., Weber, U., Ichii, K., Gans, F., Camps-Valls, G., and Reichstein, M.: The FLUXCOM ensemble  
524 of global land-atmosphere energy fluxes, *Sci. Data.*, 6(1), 1-14, doi:10.1038/s41597-019-0076-8, 2019.
- 525
- 526 Kumar, S.V., Reichle, R.H., Koster, R.D., Crow, W.T., and Peters-Lidard, C.D.: Role of subsurface physics in the  
527 assimilation of surface soil moisture observations, *J. Hydrometeorol.*, 10, 1534-1547, doi:10.1175/2009JHM1134.1,  
528 2009.
- 529
- 530 Lucchesi, R.: File specification for GEOS-5 FP, NASA GMAO Office Note 4 (version 1.0), 63 pp. Available at  
531 <https://ntrs.nasa.gov>, 2013
- 532
- 533 McColl, K., Vogelzang, J., Konings, A.G., Entekhabi, D., Piles, M., and Stoffelen, A.: Extended triple collocation:  
534 Estimating errors and correlation coefficients with respect to an unknown target, *Geophys. Res. Lett.*, 41(17), 6229-  
535 6236, doi:10.1002/2014gl061322, 2014.
- 536
- 537 Piepmeier, J. R., Focardi, P., Horgan, K. A., Knuble, J., Ehsan, N., Lucey, J., Brambora, C., Brown, P. R., Hoffman,  
538 P. J., French, R. T., Mikhaylov, R. L., Kwack, E. Y., Slimko, E. M., Dawson, D. E., Hudson, D., Peng, J., Mohammed,  
539 P. N., de Amici, G., Freedman, A. P., Medeiros, J., Sacks, F., Estep, R., Spencer, M. W., Chen, C. W., Wheeler, K. B.,  
540 Edelstein, W. N., O'Neill, P. E., and Njoku, E. G.: SMAP L-band microwave radiometer: Instrument design and first  
541 year on orbit, *IEEE T. Geosci. Remote.*, 55(4), 1954–1966, doi:10.1109/TGRS.2016.2631978, 2017.
- 542
- 543 Liu, Q., Reichle, R., Bindlish, R., Cosh, M.H., Crow, W.T., de Jeu, R., de Lannoy, G., Huffman, G.J. and Jackson,  
544 T.J.: The contributions of precipitation and soil moisture observations to the skill of soil moisture estimates in a land  
545 data assimilation system, *J. Hydrometeorol.*, 12(5), 750-765, doi:10.1175/JHM-D-10-05000.1, 2011.
- 546
- 547 Reichle, R.H., Crow, W.T., Koster, R. D., Sharif, H. and Mahanama, S.: Contribution of soil moisture retrievals to  
548 land data assimilation products, *Geophys. Res. Lett.*, 35(1), doi:10.1029/2007GL031986, 2008.



549  
550 Reichle, R. H., de Lannoy, G. J. M., Liu, Q., Ardizzone, J. V., Colliander, A., Conaty, A., Crow, W., Jackson, T. J.,  
551 Jones, L. A., Kimball, J. S., Koster, R. D., Mahanama, S. P., Smith, E. B., Berg, A., Bircher, S., Bosch, D., Caldwell,  
552 T. G., Cosh, M., González-Zamora, Á., Holifield Collins, C. D., Jensen, K. H., Livingston, S., Lopez-Baeza, E.,  
553 Martínez-Fernández, J., McNairn, H., Moghaddam, M., Pacheco, A., Pellarin, T., Prueger, J., Rowlandson, T., Seyfried,  
554 M., Starks, P., Su, Z., Thibeault, M., van der Velde, R., Walker, J., Wu, X., and Zeng, Y.: Assessment of the SMAP  
555 Level-4 surface and root-zone soil moisture product using in situ measurements, *J. Hydrometeorol.*, 18(10), 2621–  
556 2645, doi:10.1175/JHM-D-17-0063.1, 2017a.

557  
558 Reichle, R. H., de Lannoy, G. J. M., Liu, Q., Koster, R. D., Kimball, J. S., Crow, W. T., Ardizzone, J. V., Chakraborty,  
559 P., Collins, D. W., Conaty, A. L., Giroto, M., Jones, L. A., Kolassa, J., Lievens, H., Lucchesi, R. A., and Smith, E. B.:  
560 Global assessment of the SMAP Level-4 surface and root-zone soil moisture product using assimilation diagnostics, *J.*  
561 *Hydrometeorol.*, 18(12), 3217–3237, doi:10.1175/jhm-d-17-0130.1, 2017b.

562  
563 Reichle, R. H., de Lannoy, G., Koster, R. D., Crow, W. T., Kimball, J. S., and Liu, Q.: SMAP L4 Global 9 km EASE-  
564 grid surface and root zone soil moisture land model constants, Version 4, NASA National Snow and Ice Data Center  
565 DAAC, <https://doi.org/10.5067/KGLC3UH4TMAQ>, 2018a

566  
567 Reichle, R. H., de Lannoy, G., Koster, R. D., Crow, W. T., Kimball, J. S., & Liu, Q.: SMAP L4 global 3-hourly 9 km  
568 EASE-grid surface and root zone soil moisture analysis update data, version 4, NASA National Snow and Ice Data  
569 Center DAAC, <https://doi.org/10.5067/60HB8VIP2T8W>, 2018b

570  
571 Reichle, R. H., de Lannoy, G., Koster, R. D., Crow, W. T., Kimball, J. S., & Liu, Q.: SMAP L4 global 3-hourly 9 km  
572 EASE-grid surface and root zone soil moisture geophysical data, version 4, NASA National Snow and Ice Data Center  
573 DAAC, <https://doi.org/10.5067/KPJNN2GI1DQR>, 2018c

574  
575 Reichle, R. H., Liu, Q., Koster, R. D., Crow, W. T., De Lannoy, G. J., Kimball, J. S., and Kolassa, J.: Version 4 of the  
576 SMAP Level-4 soil moisture algorithm and data product, *J. Adv. Model Earth Sy.*, 11(10), 3106-3130,  
577 doi:10.1029/2019MS001729, 2019.

578  
579 Seneviratne, S. I., Corti, T., Davin, E. L., Hirschi, M., Jaeger, E. B., and Lehner, I.: Investigating soil moisture–climate  
580 interactions in a changing climate: A review, *Earth-Sci. Rev.*, 99, 125–161, doi:10.1016/j.earscirev.2010.02.004, 2010.

581  
582 Seneviratne, S. I., Wilhelm, M., Stanelle, T., Hurk, B., Hagemann, S., and Berg, A.: Impact of soil moisture-climate  
583 feedbacks on CMIP5 projections: First results from the GLACECMIP5 experiment, *Geophys. Res. Lett.*, 40(19), 5212–  
584 5217, doi:10.1002/grl.50956, 2013.

585



- 586 Shen, Y., Xiong, A., Wang, Y., and Xie, P.: Performance of high-resolution satellite precipitation products over China,  
587 J. Geophys. Res.-Atmos., 115(D2), doi:10.1029/2009JD012097, 2010.
- 588
- 589 Shen, Y. and Xiong, A.: Validation and comparison of a new gauge-based precipitation analysis over mainland China,  
590 Int. J. Climatol., 36(1), 252-265, doi:10.1002/JOC.4341, 2015.
- 591
- 592 Verger, A., Baret, F., and Weiss, M.: Performances of neural networks for deriving LAI estimates from existing  
593 CYCLOPES and MODIS products, Remote Sens. Environ., 112, 2789-2803, doi:10.1016/j.rse.2008.01.006, 2008.
- 594
- 595 Xie, P., Yatagai, A., Chen, M., Hayasaka, T., Fukushima, Y., Liu, C., and Yang, S.: A gauge-based analysis of daily  
596 precipitation over East Asia, J. Hydrometeorol., 8, 607-626, doi:10.1175/JHM583.1, 2007.
- 597
- 598 Xie, P., Joyce, R., Wu, S., Yoo, S.-H., Yarosh, Y., Sun, F., Lin, R.: NOAA CDR Program: NOAA Climate Data  
599 Record (CDR) of CPC Morphing Technique (CMORPH) High Resolution Global Precipitation Estimates, Version 1.  
600 NOAA National Centers for Environmental Information, 2019.